Interfactant-mediated quasi-Frank–van der Merwe growth of Pb on Si(111)

Th. Schmidt* and E. Bauer†
Physikalisches Institut, Technische Universität Clausthal, 38678 Clausthal-Zellerfeld, Germany
(Received 8 December 1999; revised manuscript received 5 June 2000)

The influence of interfactants (Au, Ag) on the growth of Pb on Si(111) is studied by low-energy electron microscopy in the temperature range from 260 K to 460 K. On the Si(111)-(7×7) surface Pb grows in the Stranski–Krastanov mode, on the Si(111)-($\sqrt{3}\times\sqrt{3}$)R30°-Au and on the Si(111)-(6×6)-Au surface in the quasi-Frank–van der Merwe (layer-by-layer) mode. On the Si(111)-($\sqrt{3}\times\sqrt{3}$)R30°-Ag surface the growth mode changes from layer-by-layer below 300 K to the Stranski–Krastanov mode above 300 K. The temperature dependence of the growth cannot be explained by thermodynamics but is governed by kinetics. The analysis of the maximum island density in terms of the atomistic nucleation theory gives acceptable values for nucleus size and energies only in the layer-by-layer growth regime. In the Stranski–Krastanov growth regime abnormal values are obtained that are attributed to high cluster mobility on the initial two-dimensional layer. The conditions leading to quasi-Frank–van der Merwe growth are discussed.

I. INTRODUCTION

Metal overlayers are important both in technology and science. For example, semiconductor technology requires a multitude of metal films for contacts, diodes, or interconnects. The structure of the film has a significant influence on the reliability of devices. In basic science films that are only a few or even only 1 monolayer (ML) thick are of special interest, because their properties differ drastically from those of the bulk due to the reduced dimensionality and due to the interaction with the substrate. Such ultrathin films can be grown only under very specific conditions. The goal of the present paper is to obtain an understanding of a submicroscopic basis of one of the methods—to be discussed below—which allows to soften these conditions, so that a wider range of film-substrate combinations becomes accessible to quasi-two-dimensional layer growth.

More than 40 years ago one of us classified the growth of thin films on the basis of thermodynamical considerations in three modes:[1] Frank–van der Merwe (FM), Stranski-Krastanov (SK), and Volmer–Weber (VW) [Figs. 1(a)–1(c), respectively], depending upon the energy balance $\Delta\sigma=\sigma_A+\sigma_I-\sigma_S$ of the surface free energies σ_A of the adsorbate A, σ_I of the interface I, and σ_S of the substrate S. In the case where $\Delta\sigma<0$, pure two-dimensional (2D) growth is energetically favored [Fig. 1(a)]. When $\Delta\sigma>0$, pure three-dimensional (3D) growth is favored. Between these two modes, the SK mode is situated: the film starts to grow in the FM mode ($\Delta\sigma<0$), whereas after one or several layers the relation in the energy balance changes such that $\Delta\sigma>0$ and 3D growth is preferred. The basic factors that determine these different growth behaviors are of elastic and electronic origin, i.e., (i) the strain in the film due to lattice mismatch (different lattice constants and/or different lattice structures) and (ii) the chemical bonding between film and substrate. Both factors are subsumed in σ_I. Ideal FM growth can occur, therefore, only in homoepitaxy.

For a given film-substrate combination σ_A, σ_I, and σ_S are fixed and, therefore, also $\Delta\sigma$. If $\Delta\sigma\geqslant 0$, it can be made negative, however, by involving a third component in the growth process, either by reducing σ_A with a surface energy-reducing adsorbate A*, called *surfactant* [Fig. 1(d)] or by reducing σ_I with an interface energy-reducing layer I*, which is more strongly bound to the substrate than the film to be grown, called *interfactant* [Fig. 1(e)]. The first method was introduced by Copel *et al.*[2] in the growth of Ge on Si(001), the second by Jałochowski and Bauer[3] in the growth of Pb on Si(111). Surfactants have been the subject of many submicroscopic studies[4] in the meantime, which have lead to a basic understanding of the processes involved. For the second method such studies and the understanding derived from them are still missing. This is the motivation for the present paper on the film/substrate system Pb/Si(111) with Au and Ag as third components that have been found to be effective interfactants.[5,6] The lattice constants of Pb ($a_{\mathrm{Pb}}=4.95$ Å) and Si ($a_{\mathrm{Si}}=5.43$ Å) differ significantly, leading to a 9% lattice mismatch. Numerous studies have shown that Pb grows on Si(111) in the SK mode.[7–11] The initial 2D layer is incommensurate (IC) when grown at low temperatures, for example at room temperature but has a ($\sqrt{3}\times\sqrt{3}$)R30° structure when deposited or annealed at elevated temperatures.[9–16]

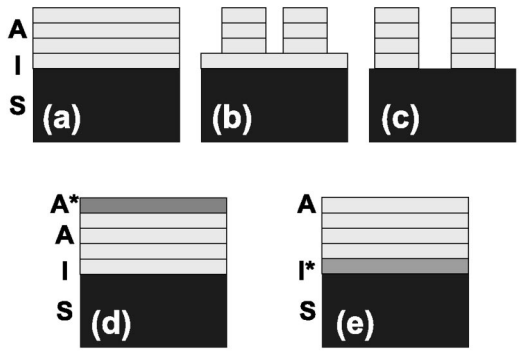

FIG. 1. Growth modes in the epitaxy: (a) Frank–van der Merwe, (b) Stranski–Krastanov, and (c) Volmer–Weber and possible influence on the growth by (d) a surfactant and (e) an interfactant. A = adsorbate, I = interface, S = substrate, A* = surfactant, and I* = interfactant.

II. EXPERIMENTAL SETUP AND PROCEDURES

The surface of the silicon wafers used in this paper deviated less than 0.04° from the (111) orientation. This miscut corresponds to an average step distance of about 500 nm but areas with step distances larger than 1 μm could be found on the sample. The chemically oxidized Si(111) sample was outgased at about 1000 K for about 24 h and finally flashed to about 1400 K to remove the oxide film at a pressure below $p=3\times10^{-9}$ mbar. The cleanness of the surface can be judged by observing the phase transition using low-energy electron microscopy (LEEM). This phase transition is very sensitive to contamination.[17] The temperature of the sample was measured with a W5%Re–W26%Re thermocouple attached to the sample holder. The melting points of three-dimensional Pb islands (601 K) and the $(7\times7)\leftrightarrow(1\times1)$ phase transition at 1110 K (Ref. 17) were used for its calibration.

The experiments were carried out in a precursor instrument of a commercial LEEM (Ref. 18). The instrument and the method are described in Ref. 19. Sample cooling to temperatures below room temperature was achieved by connecting the specimen holder via isolation stand offs and a copper braid to a liquid-nitrogen cold finger. This allowed us to reach temperatures of 260 K at the sample, which is at high voltage (18 kV) without impairing the possibility of heating to more than 1800 K during observation. The base pressure in the specimen chamber was $p=1.0\times10^{-10}$ mbar. Pb, Ag, and Au were evaporated from three Knudsen cells. The deposition rates and pressures during deposition were 0.5 ML/min at 1.4×10^{-10} mbar (Pb), and 0.2 ML/min at 5×10^{-10} mbar (Ag and Au). The monolayer (ML) Pb is defined as the atomic density of the Pb(111) plane (1 ML $=9.43\times10^{14}$ atoms/cm^2), except when Pb superstructures on Si(111) are discussed, in which case 1 ML$=7.83\times10^{14}$ atoms/cm^2 is the atomic density of the unreconstructed Si(111) surface. The latter definition is used for the Ag and Au ML as well. The rates were determined by the completion of known superstructures (Ag, Au) and by the island formation period during the FM growth of Pb on the Si(111)-(7×7) surface. The accuracy of this calibration is about 3%. A typical energy for imaging Pb films on the Si(111) surface is 8 eV. This gives good step contrast as well as high intensity. All experiments are video recorded and subsequently frame grabbed. This procedure is always connected with some loss of image quality.

III. RESULTS

A. Overview of the growth with different interfactants

Before discussing the results in detail, a brief overview of the effect of interfactants will be given using a 5 ML thick Pb film deposited at $\approx$270 K, except for the deposition onto the Si(111)-$(\sqrt{3}\times\sqrt{3})$R30°-Ag surface (in the following: Ag-$\sqrt{3}$), which was made at 288 K (Fig. 2). The imaging conditions, i.e., kinetic energy (8 eV), magnification, and focusing conditions, are about the same. Figure 2(a) shows a Pb film grown on the clean Si(111)$-(7\times7)$ surface at 273 K. The film still has many elongated holes (dark regions). The original Pb islands are interconnected and monoatomic steps on the Pb(111) islands are visible. About 75% ($\pm2\%$) of the substrate is covered by these Pb islands. The growth is different when the first 0.46–0.58 ML (that is 0.55–0.69 ML in Si units) is deposited at 430 K, which converts the Si(111)$-(7\times7)$ surface into the Si(111)-$(\sqrt{3}\times\sqrt{3})$R30°-Pb surface (in the following Pb-$\sqrt{3}$) after slow cooling. The further deposition of 5 ML of Pb is made after cooling to 274 K [Fig. 2(b)]. Now the Pb islands are much larger compared to the growth on the clean Si(111)-(7×7) surface, but the holes are larger, too. A slightly higher percentage of only 80% ($\pm2\%$) of the substrate is covered by thick flat Pb islands with many monolayer terraces, the rest is the Pb-$\sqrt{3}$ surface. A quite different growth mode is observed when Pb is deposited onto a Ag-$\sqrt{3}$ surface that had been prepared at 830 K [Fig. 2(c)]. Now the Pb film grown at 288 K is perfectly closed, the surface is nearly perfectly flat. This is an example of the interfactant mediated FM growth. The next interfactant candidate is gold, which forms three kinds of superstructures on the Si(111) surface: the (5×2)-Au, the $(\sqrt{3}\times\sqrt{3})$R30°-Au , and the (6×6)-Au structure. On the Si(111)-(5×2)-Au surface Pb grows at 273 K in the SK mode with elongated holes that extend down to the 1 ML covered substrate, and covers at 5 ML about 89% ($\pm2\%$) of the surface [Fig. 2(d)]. On the Au-$\sqrt{3}$ surface at 269 K [Fig. 2(e)] and on the Si(111)-(6×6)-Au surface at 267 K [Fig. 2(f)] Pb grows in the quasi-FM mode. The azimuthal orientation of all Pb layers with the exception of the layer grown on the (6×6)-Au surface is parallel to the substrate; on the (6×6) surface it is rotated by 30°. In the following we discuss the growth on four of these superstructure in detail.

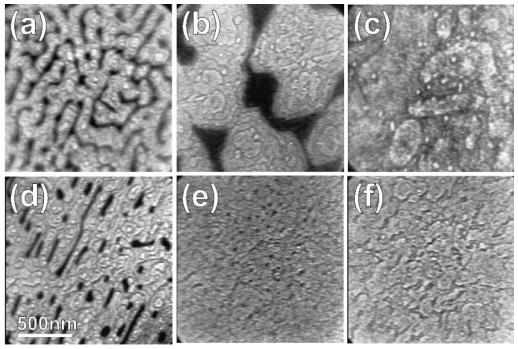

FIG. 2. LEEM images of 5 ML thick Pb films grown on various Si(111) surfaces at 270 K. Electron energy 8 eV (a) (7×7), (b) Pb-$\sqrt{3}$, (c) Ag-$\sqrt{3}$, (d) (5×2)-Au, (e) Au-$\sqrt{3}$, and (f) (6×6)-Au.

B. Pb/Si(111)-(7×7)

When deposited at 273 K and 290 K (room temperature) the first Pb layer, as judged by the appearance of the second layer islands, is completed at 0.77 Pb-ML. The first layer is incommensurate with the substrate in agreement with earlier studies in which a saturation coverage of 1 ML in Si(111) units (0.83 Pb-ML) was reported.[16] With increasing substrate temperature the second layer islands appear at lower coverages, for example at 350 K at 0.67 Pb-ML, that is at 0.80 ML in the Si(111) density units used here. This temperature dependence of the second layer nucleation is shown in Fig. 3(a).

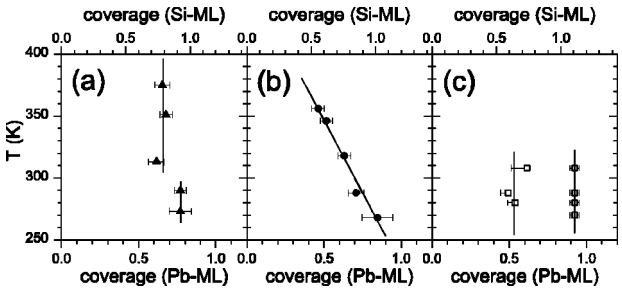

FIG. 3. Saturation coverage of the first Pb layer grown on the (a) Si(111)-(7×7), (b) Ag-$\sqrt{3}$, and (c) (6×6)-Au surface.

The growth at 290 K on the first layer is shown in Fig. 4, which is a series of images taken during deposition. The step structure of the substrate is indicated on the left-hand side. The surface rises from the left to the right. In the left image, 1.1 ML Pb has been deposited. The first closed layer appears dark in LEEM at the chosen energy. The bright Pb islands on top of this layer are 1 ML thick. Nucleation is preferred at the lower level of the substrate steps. The density of islands is determined in this early stage of growth and changes in the following only due to agglomeration of islands. The islands grow only slowly laterally upon further deposition. After deposition of 2 ML (middle image of Fig. 4) the islands still cover only about 50% of the surface but have now many nuclei on top. The islands on the substrate terraces are still isolated whereas the islands at the step edges have grown together nearly completely and now start to grow over the substrate steps. At a coverage of 6 ML about 80% of the substrate is covered by islands most of which have grown together with others. Also, the shape of the islands has changed from round to more or less hexagonal.

In order to have a more detailed view, Fig. 5 shows the square region in the middle of Fig. 4 at higher magnification in steps of 0.23 ML in the thickness range from 3.1 to 5.0 ML. In the lower right of each image there is a substrate step edge below the Pb island—indicated by the dashed line in the 3.08 ML image—which causes elongated terraces on the islands parallel to the step. In contrast to this, the terraces on the islands on the substrate terraces are round. New terraces—indicated by arrows—nucleate mostly in the center of a terrace before the terrace edge reaches the border of the island. However, multiple nucleation off the center followed by coalescence—compare, for example the lower-left parts of the 4.31 and 4.54 ML images—is also quite frequent. In the coverage range shown the islands start to become hexagonal and to grow together (see the example in the circles). The lowest terraces seen in these images are already several monolayers thick. The side faces are too steep as to allow resolution of the single terrace sequence but the transition

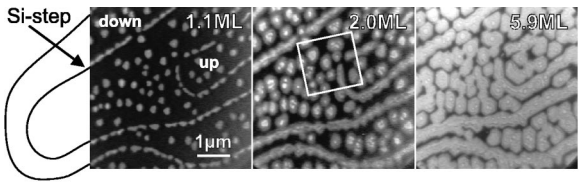

FIG. 4. Growth of Pb on the Si(111)-(7×7) surface at 290 K. Electron energy 8 eV.

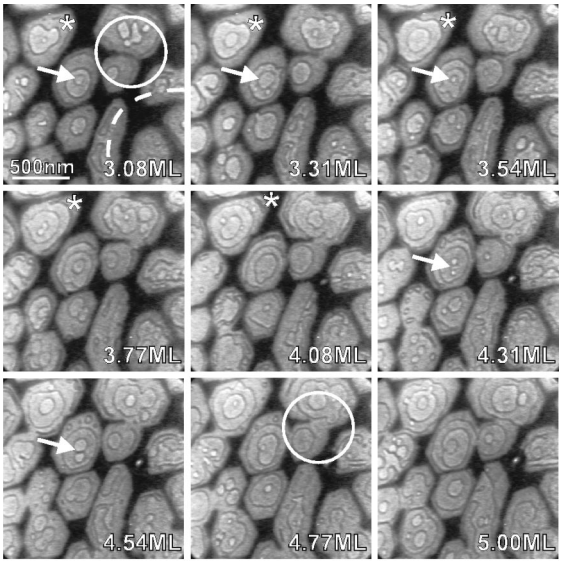

FIG. 5. Growth of Pb on the Si(111)-(7×7) surface at 290 K between 3 and 5 ML. Electron energy 8 eV. For explanation see the text.

from incomplete to complete terrace on top of the islands can be seen quite well in the upper left in the images between 3.08 and 4.08 ML indicated by asterisks.

Decreasing the deposition temperature causes a drastic increase of the island density by about two orders of magnitude in a temperature range of only 100 K. In Fig. 6(a) 2 ML of Pb were deposited at different temperatures. At the substrate step density in these images (step distance ≈ 1 μm) the decoration of Si steps occurs at 290 K and 313 K. At lower and higher temperatures they have no influence. The islands are round at the two lower temperature ranges. At the two higher temperatures they have irregular shape.

The coverage dependence of the island density is shown in a double-logarithmic plot in Fig. 6(b) for the three higher temperatures of Fig. 6(a). θ^* is the coverage in excess of the first monolayer. The completion of the first monolayer can only be determined with an accuracy of 2 s at a deposition

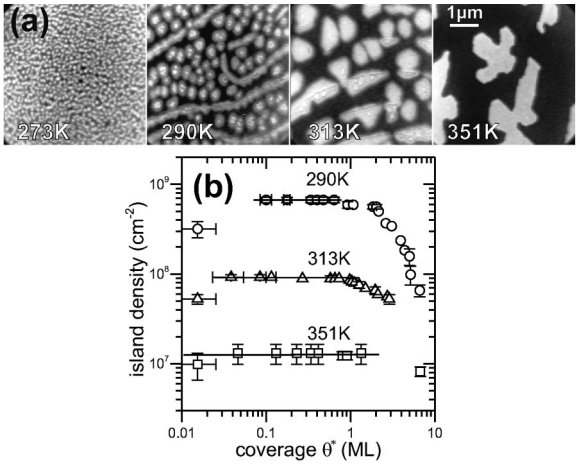

FIG. 6. Growth of Pb on the Si(111)-(7×7) surface. (a) Temperature dependence at a total coverage of 2 ML Pb in all images. (b) Coverage dependence of the 3D island density on the first Pb monolayer, θ^* is the coverage in excess of the first monolayer. The horizontal lines are a guide for the eyes.

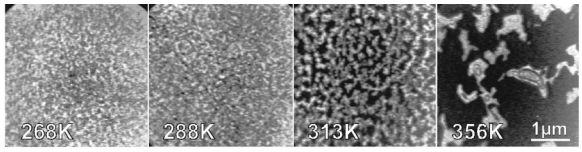

FIG. 7. Temperature dependence of the growth of Pb on the Si(111)-($\sqrt{3}\times\sqrt{3}$)R30°-Ag surface at a total coverage of 2 ML Pb.

rate of 1 ML/130 s. It is evident that additional nucleation between the first and second data point occurs only at 290 K and 313 K, while at 351 K, the island density is constant within the limits of error over a wide coverage range up to about $\theta^*=0.5-0.6$ ML, similar to 290 K and 313 K, where it is constant after the first data point. Agglomeration occurs only above about $\theta^*=0.7$ ML. This allows an analysis of the island density at about $\theta^*=0.1-0.5$ ML in terms of the maximum island density as suggested by Venables,[20,21] in view of the fact that the nucleation stage is not accessible to LEEM (see Sec. IV A).

C. Pb/Si(111)-($\sqrt{3}\times\sqrt{3}$)-Ag

The Si(111)-($\sqrt{3}\times\sqrt{3}$)R30°-Ag surface was prepared by depositing Ag onto the (7×7) surface at temperatures between 675 K and 835 K until the layer was completed as seen by the disappearance of the last (7×7) regions in LEEM. Subsequently the crystal was cooled slowly (in about 20 to 60 min) to the Pb deposition temperature, which ranged from 268 K to 356 K.

The saturation coverage of the first (2D) Pb layer as determined from the appearance of the first second layer islands depends linearly on the deposition temperature and covers the range of $0.5-0.9$ ML at the investigated temperatures [Fig. 3(b)]. At 288 K the first layer is completed after deposition of 0.7 ML Pb, that is at a coverage of 5/6 ML in Si(111) density units. At 318 K this layer has a (6×1) LEED pattern, which suggests that the layer consists of three well-ordered domains in which every sixth Pb atom along the $\langle 11\overline{2}\rangle$ direction is missing. Most likely the Pb atoms are on top of the saturated Ag layer because no 2D Ag particles are seen that would be formed when Ag atoms are displaced by incorporation of Pb into a mixed layer, a phenomenon which has been observed when 0.7 ML Au [in Si(111) density units] are deposited onto the Ag-$\sqrt{3}$ layer.[22] The difference is not surprising because the Au–Si bond is much stronger (3.65 eV/atom)[23] than the Ag–Si bond (2.82 eV/atom)[23] while the Pb–Si bond is weaker (2.65 eV/atom).[9]

The nucleation rate on top of this first Pb layer is much higher than in the case of Pb on top of the first Pb layer on the (7×7) surface. The temperature dependence of the structure of the layer after deposition of a total amount of 2 ML Pb is shown in Fig. 7. At this coverage the islands have already grown together to a large extent, which leads to the irregular shape seen above 300 K. At 313 K only 50% of the surface is covered by islands, at 356 K only 20% so that they are on average about 2.5 ML $[=(2-0.7)/0.5]$ or 6.5 ML $[=(2-0.7)/0.2]$ thick. Below 300 K the substrate is nearly completely covered with the second Pb layer. The maximum of the island density occurred at all temperatures at a total coverage of about 1 ± 0.1 ML. It will be evaluated at this coverage in Sec. IV as described in Sec. III B.

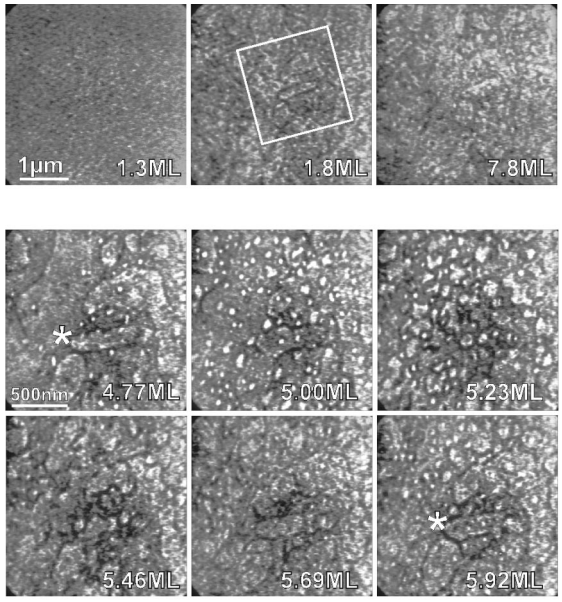

FIG. 8. Growth of Pb on the Si(111)-($\sqrt{3}\times\sqrt{3}$)R30°-Ag surface at 288 K. Electron energy 8 eV. The lower images show a magnified part of the square in the middle-upper image. The asterisks indicate the same point on the surface.

Figure 8 shows the FM growth of Pb on the Ag-$\sqrt{3}$ surface at $T=288$ K. During the preparation of the Si(111)-($\sqrt{3}\times\sqrt{3}$)R30°-Ag the (7×7) superstructure must be transformed. In this process many Si adatoms are set free, which rearrange the existing Si steps and nucleate new islands on the terraces. For this reason the Ag-$\sqrt{3}$ substrate has a higher step density than the pure Si(111)-(7×7) substrate (see also Ref. 24). The same was observed with scanning tunnel microscopy (STM) during the growth of Pb on the pure Si(111)-(7×7) and on the Ge(111) surface, deposited at room temperature and annealed to 100°C.[15] During the growth of Pb on the surface, these steps are reproduced by the Pb film, which is otherwise nearly completely flat, as illustrated in the upper part of Fig. 8. In its lower part the growth in the region of the square in the center-upper image is shown with higher magnification and higher resolution. At 4.77 ML nucleation starts on a closed and flat Pb film. The coverage has a fractional value because the first Pb layer has a thickness of only 0.7 ML. The small bright circles are the newly formed islands whereas the larger step structure is due to the morphology of the Ag-$\sqrt{3}$ surface, as discussed before. New nuclei are formed still up to 5.23 ML, while the previously formed terraces have already grown laterally and coalescence occurs. Subsequently the layer starts to close and the process repeats itself. The image at 5.92 ML is very similar to that at 5.00 ML except for a slight change of focus.

D. Pb/Si(111)-(6×6)-Au

The Si(111)-(6×6)-Au surface is prepared in two steps: (1) deposition of Au at 800 K, which leads to a well-ordered (5×2) structure followed by the ($\sqrt{3}\times\sqrt{3}$) structure.[25,26] When this structure is completed, which can be clearly seen in LEEM, the Au deposition is interrupted. (2) After cooling to 590 K, deposition is continued until a well-ordered (6×6) structure is obtained. Similar to the preparation of the

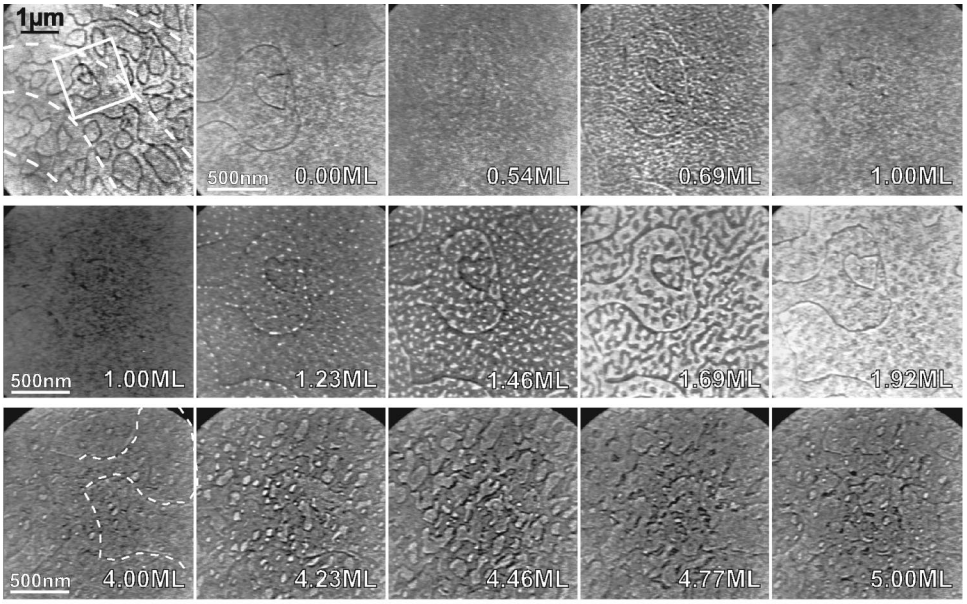

FIG. 9. Growth of Pb on the Si(111)-(6×6)-Au surface at 280 K. The left-top image shows the initial (6×6)-Au surface at lower magnification; the dashed lines indicate the substrate step position before the Au deposition. Electron energy 8 eV.

Ag-$\sqrt{3}$ structure, the Si(111) surface becomes laterally rougher during the growth of the (5×2)-Au and Au-$\sqrt{3}$ structure. In the left-top image of Fig. 9 the Si(111)-(6×6)-Au surface is shown. The substrate step position before the Au deposition is roughly indicated by the dashed lines. This change of the morphology is due to the Si adatoms, which are set free during the transformation from the (7×7) to the (5×2) structure[27,28] and during the following transformations to the $(\sqrt{3}\times\sqrt{3})$ and (6×6) structures; Seehofer[29] reported that the growth of Si(111)-(5×2)-Au on vicinal Si(111) surfaces can even induce faceting of the surface.

The topmost row of Fig. 9 shows the growth of the first monolayer in the magnified region of the first image indicated by a white square. The intensity of each image is scaled for optimized contrast. The image at 0.0 ML shows the pure Si(111)-(6×6)-Au surface with substrate steps. The surface rises from the left to the right-hand side. Deposition of Pb on this surface at 280 K decreases contrast and resolution up to a coverage of about 0.5 ML either due to statistical incorporation of Pb or due to growth of small unresolved domains with $\sqrt{3}\times\sqrt{3}$ structure, which is seen in this coverage range in LEED. Upon further deposition the substrate step contrast appears again and islands can be observed with a typical distance of about 50 nm (white spots at 0.69 ML in Fig. 9). These islands nucleate preferentially at the lower side of the substrate step edge. At 0.92 ML the islands have grown together to cover the surface completely. The saturation coverage of the first closed layer at about 0.5 ML (defined by the first visible islands) and of the closed layer at 0.92 ML is plotted in Fig. 3(c) for various deposition temperatures. The LEED pattern at 1 ML is that of the Pb(111) surface rotated 30° relative to the Si(111) substrate, in agreement with earlier work.[30] The transition from the (6×6)-Au to the Pb(111)-(1×1)R30° structure may be envisaged as follows. Adsorption of Pb disorders the (6×6)-Au superstructure of the $(\sqrt{3}\times\sqrt{3})$R30°-Au structure, perhaps in a manner similar to the corresponding thermal disordering of the (6×6)-Au structure. Ideally the process could be but must not be completed at 1/3 ML Pb [in Si(111) units], for example by adsorption of one Pb on top of the Au trimers of the $(\sqrt{3}\times\sqrt{3})$R30°-Au structure. Above this coverage, Pb(111)$-(1\times1)$R30° islands form in the $(\sqrt{3}\times\sqrt{3})$R30°-(Au, Pb) sea, incorporating the Pb atoms in the sea until the islands have grown together to a complete first Pb(111) monolayer with reduced density [0.92 ML in Pb(111) units]. In reality, due to local coverage fluctuations and perhaps preferred nucleation sites, the Pb(111) nucleation may set in earlier and the $(\sqrt{3}\times\sqrt{3})$R30°-Au +Pb structure may be completed later than at 1/3 Si-ML. This would imply that nucleation sets in long before islands can be resolved in LEEM and suggests the possibility that the nucleation density may be much higher than the island density seen at 0.69 ML, which may already be a consequence of coalescence. Another possibility is a $(\sqrt{3}\times\sqrt{3})$R30° structure with two Pb atoms per unit cell. In this case the structure is completed at 2/3 ML in Si units, that is 0.55 ML in Pb units. Shortly before this coverage the first nuclei of the Pb(111)-(1×1)R30° islands are formed. This structure model also assumes that nucleation sets in before the $(\sqrt{3}\times\sqrt{3})$R30°-(Au, Pb) structure is completed.

The Pb(111)-(1×1)R30° structure destroys the underlying $(\sqrt{3}\times\sqrt{3})$R30°-(Au, Pb) structure, perhaps by converting it into a (1×1), a disordered, or even a structure with the same periodicity as the Pb layer. LEEM does not allow a distinction between these possibilities and LEED studies were not made in sufficient detail to answer this question or to determine the lattice constant of the Pb layer precisely. From the value of the saturation coverage of 0.92 ML, the lattice constant of the Pb monolayer can be calculated as 5.16 Å, which is clearly incommensurate with the substrate. However, the first nucleation of the second layer occurs at 1.0 ML. Possibly, in the coverage range from 0.92 to 1.0 ML, additional Pb adatoms form a 2D gas or are incorporated into the first monolayer, which is thus compressed from the lattice constant 5.16 Å to the bulk value 4.95 Å .

The second row in Fig. 9 shows the growth of the second Pb layer. Due to reflectivity differences the first layer appears dark, the second layer bright. The islands of the second layer nucleate first at the lower edge of the substrate steps (1.23

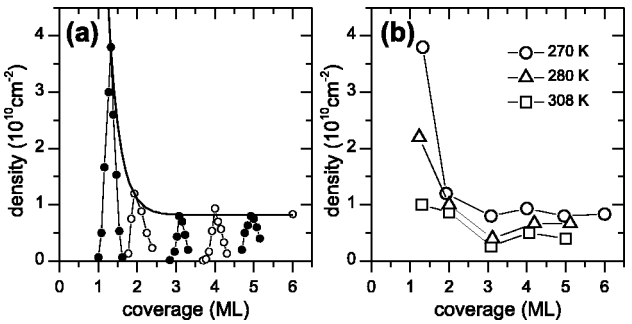

FIG. 10. 2D island density during the growth of Pb on the (6 ×6)-Au surface at 270 K (a) and the coverage dependence of the maxima at different temperatures (b). The solid curve in (a) is a guide for the eye.

ML) and afterwards on the substrate terraces (1.46 ML). At 1.46 ML the average distance of nuclei is about 60 nm and many of them have already coalesced, in particular at the steps, where agglomeration is nearly completed. At 1.69 ML all islands on the surface steps have grown together. The holes in between are elongated and of irregular shape. In particular the upper side of the substrate steps is not covered by the second Pb layer, indicating that all Pb adatoms are captured by the Pb island at the lower side of the step. At 1.92 ML the second layer is nearly completely filled. A few nuclei of the third layer and small holes in the second layer can be seen (bright- and dark-gray dots in the 1.92 ML image in Fig. 9). Due to this quasiperfect FM growth, the step structure of the substrate is reproduced in the Pb layer, which is clearly seen by comparing the 0.0 ML image with the 1.92 ML image in Fig. 9. During the growth of the second and the following layers the LEED pattern is always a Pb(111)-(1 ×1)R30°. This means that the orientation and the lattice constant do not change within the limits of error.

Even at higher coverages Pb grows nearly in an ideal FM mode (bottom row in Fig. 9). At 4.0 ML the first islands of the fifth layer are visible. Fresnel diffraction due to slight defocusing makes these small islands appear brighter. It is possible to recognize the step structure of the substrate (dashed line, compare with the upper rows in Fig. 9), which indicates the perfection of the growth. At 4.23 ML the nucleation process of the fifth layer is completed. Reproduced substrate steps are no longer preferred nucleation sites. The islands grow together, leaving some elongated holes at 4.77 ML (dark areas in the image). At 5.0 ML the nucleation of the sixth layer has already started (bright islands) before the fifth layer is completely closed (dark holes). This slight deviation from the ideal FM growth generally causes the damping of RHEED oscillations. When the fifth monolayer is closed the step structure of the substrate is nearly recovered.

The density of 2D Pb islands during the growth of Pb on the (6×6)-Au at 270 K is plotted in Fig. 10(a). The first second Pb monolayer islands appear at 1.0 ML and nucleation continues up to 1.3 ML. Afterwards the island density decreases because of coalescence. In principle this process is repeated in the following layers, but nucleation starts at about 0.2 ML before completion of the monolayer and the maximum density occurs at the full monolayer. Clearly the nucleation rate at 1 ML is the highest, followed by that at 2 ML. At 0.5 ML the nucleation rate is so high, that it cannot be determined accurately. This coverage dependence of the maxima is nearly the same in the investigated temperature range, as can be seen in Fig. 10(b), except for a lower density at higher temperature. The temperature dependence of the maximum island densities at 1 ML and those at 3 ML, which represents the quasihomoepitaxial growth of Pb(111) will be shown and discussed in Sec. IV A.

E. Pb/Si(111)-($\sqrt{3}\times\sqrt{3}$)-Au

In the investigated lower temperature range ($\leqslant$300 K) Pb grows on the Au-$\sqrt{3}$ surface in the FM mode. The growth is very similar to that on the (6×6)-Au surface. The island density is comparable to that on the (6×6)-Au surface. The main difference is the orientation of the closed Pb(111) film; it is oriented parallel to the substrate, whereas the Pb(111) film on the (6×6)-Au surface is rotated 30° with respect to the substrate. This difference must have its origin in the special structure of the submonolayer, which unfortunately was not determined.

Additional experiments were carried out at higher temperatures ($\geqslant$400 K), where Pb grows in the SK mode. The maximum density of 3D islands that start to nucleate at about 0.5 ML will be shown an discussed in Sec. IV. In between the 3D islands the Pb layer has a ($2\sqrt{3}\times 2\sqrt{3}$)R30° structure. The same structure appears when a closed, about 5 ML thick Pb film deposited at low temperature on the Au-$\sqrt{3}$ or on the (6×6)-Au surface is annealed at $\approx$500 K so that most of the Pb contracts into a few large 3D crystals.

IV. DISCUSSION

A. Island density

The 3D island density in the SK growth, and the 2D island density of the second (e.g., at 1 ML) and the fourth layer (at 3 ML) in the FM growth, are plotted in Fig. 11 as closed and open symbols, respectively. We will now analyze the five Arrhenius lines in the usual manner in terms of the atomistic nucleation theory in the form given by Venables[20,21] for complete condensation, that is negligible re-evaporation. In this approximation the maximum island density is given by

$$n_x \approx N_p(R)\exp(E_n/kT) \tag{1}$$

with N_p and E_n given by

$$N_p(R) = f(Z_0,i)(4R/N_0\nu_d)^p N_0, \tag{2}$$

$$E_n = (E_i + iE_d)/(i+2) \tag{3}$$

with N_0 being the substrate atomic density, R the deposition rate, f a function of the fraction Z_0 of the surface covered by islands at their maximum density, and i the size of the critical cluster. E_i is the binding energy of the critical cluster, ν_d and E_d the attempt frequency and the activation energy for surface diffusion. The exponent is given by $p=i/(i+2)$.

A least-square fit to the temperature dependence of Eq. (1) results in the five straight lines in Fig. 11 (solid for SK, dashed for FM growth). The two resulting fit parameters N_p and E_n are listed in Table I for the different substrates. They differ clearly in the two growth modes. The E_n values in the

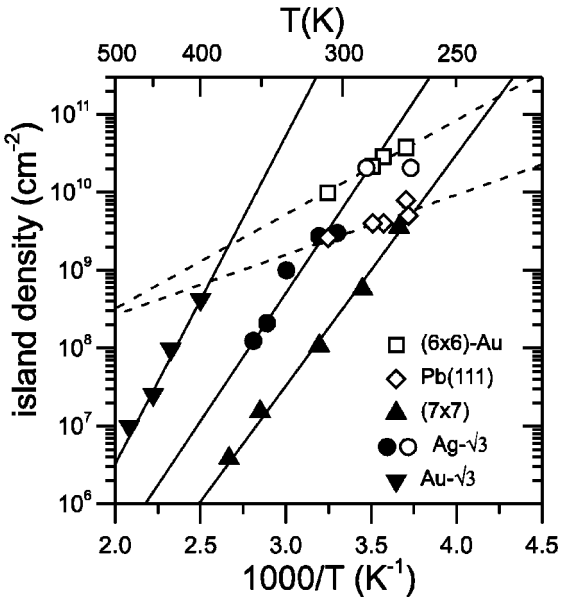

FIG. 11. Arrhenius plot of the maximum island density on the first Pb monolayer in the Si(111)-(7×7) , Ag-$\sqrt{3}$, Au-$\sqrt{3}$, and (6×6)-Au systems and on Pb(111) [= closed 3 ML thick Pb film on (6×6)-Au]. Open symbols for FM growth, full symbols for SK growth.

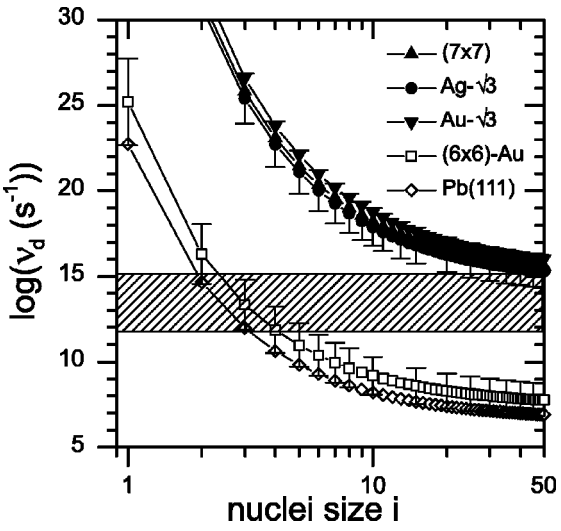

FIG. 12. Dependence of ν_d on the critical nucleus size i based on the experimental fit parameter N_p.

SK growth are three to four times larger than those of the FM growth. Because E_n/k is the slope of the Arrhenius line this can be seen as steep and flat increase in Fig. 11. On the other hand, the N_p values in the FM growth are about eight orders of magnitude larger than those in the SK growth. The N_p and E_n values in the SK growth mode are similar to those reported for quite different systems, Ag on Si(100), Si(111), W(110), and W(100).[20]

From N_p the critical cluster size can be estimated by requiring ν_d to have a physically acceptable value ($10^{12}-10^{15}$ s^{-1}) and by assuming a realistic value for the function $f(Z_0,i)$ which is usually[20,21] not far from 1, the value chosen here so that the expression for ν_d simplifies to

$$\nu_d \approx 4\frac{R}{N_0}\left(\frac{N_0}{N_p}\right)^{1/p}. \tag{4}$$

Figure 12 shows the ν_d values obtained with this expression for the five systems. It is obvious that the critical clusters are very large on the Si(111)-(7×7), Ag-$\sqrt{3}$, and Au-$\sqrt{3}$ surface ($i>20$), whereas $i\approx 2-4$ fulfills the conditions for the Pb(111) and the (6×6)-Au systems.

From E_n the activation energy for surface diffusion E_d can be estimated by making reasonable assumptions about the binding energy E_i of the critical cluster. In a simple pairwise bonding model a rough number can be obtained from the heat of sublimation $\Delta H_s = 2.02$ eV/atom[31] of Pb, which corresponds to the binding energy of a kink site. On a hexagonal surface the kink site atom has six nearest neighbors so that the energy of the Pb-Pb bond is $\Delta H/6 = 0.34$ eV/bond. For very small clusters, e.g., $i=2,3$ the bond is somewhat stronger because the bonding electrons have to be shared with fewer neighbors. Also, the bonding to the various substrates will be different from that to the Pb(111) surface causing differences in the intracluster bonding. For the estimate it is, however, sufficient to use the same value $E_i = 0.34$ eV/bond for all i and substrates, keeping in mind that the resulting E_d value is an upper limit for small i. The results are given in Table II for relevant i values, which are $i>20$ for the SK growth and $i=2-4$ for the FM growth. Fortunately the i dependence in the acceptable i ranges is negligible within the error bars, so that the diffusion energies for the adatoms on the first Pb layer of the different systems in the temperature ranges shown in Table I are 0.61 ±0.04 eV for (7×7), 0.67±0.03 eV (Ag-$\sqrt{3}$), 0.86 ±0.05 eV (Au-$\sqrt{3}$) in the SK growth mode region, 0.29 ±0.10 eV ((6×6)-Au), and 0.14±0.08 eV for Pb(111) in the FM growth mode.

TABLE I. Growth parameter of the nucleation data of Fig. 11 (SK = Stranski–Krastanov, FM = Frank–van der Merwe).

Substrate	T range (K)	Mode	$\log[N_p(\text{cm}^{-2})]$	E_n(eV)
(7×7)	273–375	SK	−1.40±0.65	0.59±0.04
Ag-$\sqrt{3}$	300–356	SK	−1.15±0.45	0.65±0.03
Au-$\sqrt{3}$	400–478	SK	−1.86±0.44	0.83±0.05
(6×6)-Au	270–310	FM	6.08±0.61	0.24±0.03
Pb(111)	270–310	FM	6.90±0.88	0.15±0.05

TABLE II. Diffusion energy of adatoms on the first Pb layer at different substrates, calculated for the acceptable i ranges.

Substrate	i range	E_d(eV) at $i=20$	$i=40$	$i=\infty$
(7×7)	⩾20	0.63±0.04	0.61±0.04	0.59±0.06
Ag-$\sqrt{3}$		0.70±0.03	0.67±0.03	0.65±0.03
Au-$\sqrt{3}$		0.90±0.06	0.86±0.05	0.83±0.03
		$i=2$	$i=3$	$i=4$
(6×6)-Au	2–4	0.31±0.06	0.29±0.10	0.28±0.05
Pb(111)		0.13±0.10	0.14±0.08	0.14±0.08

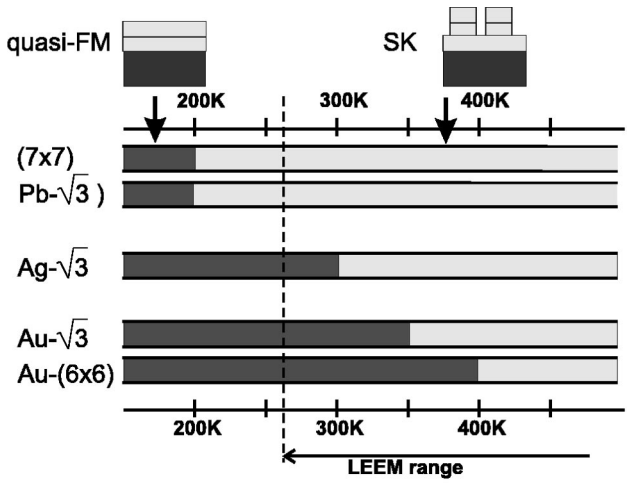

FIG. 13. Temperature ranges for Stranski–Krastanov and Frank–van der Merwe growth of Pb on the clean Si(111) surface and on different superstructures of Si(111) due to predeposition of Pb, Ag, or Au. Data for Ag-$\sqrt{3}$ and (5×2)-Au from this paper, the other data from Refs. 3 and 6.

B. Growth mode

The Ag and Au adsorption layers on Si(111) strongly modify the growth of Pb compared to the growth on the pure Si(111)-(7×7) surface. Figure 13 shows the temperature ranges of the growth modes on the various surfaces. All systems have in common that at low deposition temperatures Pb grows in the quasi-FM mode, at higher temperatures always in the SK mode. Only the transition temperature T_0 between these growth modes depends strongly on the nature of the substrate. On the clean Si(111)-(7×7) and on the Pb-$\sqrt{3}$ surface $T_0\approx200$ K (Ref. 6). Predeposition of Au shifts T_0 to higher temperatures, —the more, the higher the Au coverage: on the low coverage superstructure (5×2)-Au T_0 is just below 270 K, on the higher coverage Au-$\sqrt{3}$ structure $T_0\approx350$ K, and on the highest coverage (6×6)-Au structure $T_0\approx400$ K (Ref. 3). On the Ag-$\sqrt{3}$ the growth mode changes at 300 K. At high temperatures the systems are not far from 2D thermodynamical equilibrium, which suggests a thermodynamical interpretation as discussed in Sec. I. As a result the energy balance of the surface free energies has in all cases the same sign: $\Delta\sigma<0$ for the first layer, $\Delta\sigma>0$ at higher coverages; the absolute values can differ but the interfactant does not change the sign. As a consequence, thermodynamics cannot explain the change of the growth mode in the way suggested in the Introduction.

Therefore the growth kinetics must be responsible for the effect of the interfactant. The analysis of the experiment in terms of the atomistic nucleation theory shows that the nucleation of the SK islands is characterized by a very large size of the critical cluster ($i>20$) and a very high diffusion energy ($E_d\geqslant0.6$ eV) of the adatom on the first closed layer (Table II). Very large cluster sizes seem to be typical for SK growth systems when analyzed in terms of conventional nucleation theory. They have been reported previously for several other systems [Ag/W(110), Ag/W(100), Ag/Si(100), Ag/Si(111)].[20] Although some of these data are on good agreement with effective-medium theory calculations[32] the energies predicted by this theory differ considerably from reliable more directly determined experimental data.[33] It is difficult to reconcile at least two of the present results with the assumptions on which the conventional atomistic nucleation theory is based: (a) the strong increase of the diffusion energy in the transition from FM to SK growth with increasing temperature and (b) the earlier onset of nucleation with increasing critical cluster size and temperature on the Ag-$\sqrt{3}$ surface. Observation (b) can also not be explained by the classical phenomenological nucleation theory,[34] which should be realistic for critical cluster sizes of the order of 100 atoms. Therefore, we will stay within the framework of the atomistic nucleation theory and examine its applicability to SK growth, in particular to the systems studied in this paper.

The basic assumptions of most approximations of the atomistic nucleation theory, including the one used here, are (i) that only atoms diffuse but not dimers and larger clusters, and (ii) that no nuclei and larger clusters are lost before coalescence sets in, that is before the number of islands seen by electron microscopy decreases again. In addition, it is usually implicitly assumed that the position at which the island is observed is the nucleation site. All three assumptions have been refuted long ago in the VW growth mode.[35–37] The results of these earlier studies have been attributed to diffusion of clusters as large as 40 atoms via interfacial glide,[38] which needs little activation energy when the misfit is large.[39] Pd and Ni clusters of more than 30 atoms have been reported to float like rafts on the W(110) surface.[40] The diffusion of dimers[39] is well established by field ion microscopy, with dimer diffusion comparable or even faster than diffusion of single atoms on densely packed surfaces.[40] Recent experimental[41] and theoretical work[42,43] supports the old studies.

Zinsmeister[44] and others[45,46] have considered the influence of dimer[44–46] and trimer[45] diffusion and were able to explain at least qualitatively the discrepancies between experiment[37] and theory that takes only single atom diffusion into account. Obviously, at sufficiently low temperatures and and sufficiently high fluxes F, the effects just discussed are less likely. Diffusion of dimers has negligible influence on nucleation and growth when the diffusion constants D_1 and D_2 of monomers and dimers, respectively, obey the condition $D_2^3/D_1^2<F$ (Ref. 46). In some recent low-temperature scanning tunnel microscopy (STM) studies[47] of strongly bound adsorbates this condition was actually fulfilled. In the systems studied here in which bonding to the substrate is weak and the temperature is high, this is not the case. Although approximate solutions that take dimer and trimer diffusion into account are available,[45] they contain too many unknown parameters. Furthermore, larger clusters very likely diffuse in our experiments too. An expression similar to Eq. (1) still is expected to be valid but the quantities in this equation no longer have their original meaning. E_n cannot be separated any more in individual binding and diffusion energies but is more properly assigned to a cluster size and mobility-dependent average of these quantities. N_p now also includes some average of the entropies of the interfacial configurations.

SK growth of a material may be envisaged as VW growth

on the initial two-dimensional layer of an electronically and structurally modified form of this material. The material in excess of the initial layer does not wet it, which means that the bonding to the initial layer is weaker than that to the surface of the bulk material. Activation energies for surface diffusion of atoms, E_d, are usually proportional to the binding energy E_a, typically $E_a/10$ (Ref. 48), also for dimers and clusters. Therefore, increasing cluster migration can occur with increasing temperature causing the formation of fewer and larger islands from single atoms, dimers, and supercritical clusters. This leads to the lower maximum island density and the larger island size and E_d on the (7×7) surface covered with the ''(1×1)'' Pb monolayer than on the Pb(111) surface above 270 K. As far as dimers are concerned, the weaker bonding to the ''(1×1)'' layer than to the Pb(111) surface leaves more bonding charge within the dimer, which in the gas phase has a binding energy of 0.8 eV[49] so that the dissociation probability of the dimer should be smaller. If dimers would determine the maximum island density seen in the experiment, then it should be larger on the ''(1×1)'' layer than on the Pb(111) surface, in disagreement with our observations.

In the SK growth mode region of the Si(111)-$(\sqrt{3}\times\sqrt{3})$ R30°-Ag surface the maximum island density in the second layer is by a factor of 10 (at 400 K) to 20 (at 290 K) larger than on the Si(111)-(7×7) surface. This can be attributed to a higher nucleation rate and/or a lower cluster mobility. Figure 3(b) shows that the coverage at which the first islands appear decreases strongly with increasing temperature. Thus atoms of the first Pb layer increasingly participate in the nucleation process of the subsequent Pb growth with increasing temperature. This suggests—as does the incomplete saturation coverage of 5/6—that the Pb atoms of the first layer are weakly bound to the Ag-covered surface while the bonding between the second and first Pb layer is stronger than on the Si(111)-(7×7) surface. Therefore, the nucleation rate and cluster stability is also higher than on the Pb ''(1×1)'' layer. The difference in the temperature dependence between the various surfaces seen in Fig. 3 may also be correlated with the absence of heavy domain walls in the saturated monolayer structure of Ag[50–52] in contrast to the Pb and Au systems, which have heavy domain walls (Pb[15,16,53], Au[54]), in part with large corrugations,[55] impeding surface mobility.

The SK growth on the Au/Si surfaces was studied only on the α-Au-$\sqrt{3}$ surface. Pb interacts very strongly with the surfaces of bulk Au[56] and is expected to do so also with the Au monolayer on Si(111). This strong interaction brings the Si(111)-Au system probably close to SK growth with two stable Pb monolayers. The much higher nucleation rate of the second Pb layer compared to that of the following layers is a hint in this direction. Strong bonding to the substrate reduces surface mobility and cluster formation, leading to a large island density.

The question posed at the beginning of the paper: how does an interfactant transform the SK growth mode into a quasi-FM growth mode, can now be answered. Obviously thermodynamics cannot explain the transition because it can describe only (quasi)equilibrium phenomena. It is kinetics that drives the transition. In principle, no interfactant is necessary for quasi-FM growth of an equilibrium SK system if the temperature is low enough for high nucleation rate and negligible cluster mobility as in the case of the growth on the Si(111)-(7×7) surface. An interfactant only shifts the transition temperature to higher values by increasing the nucleation rate and decreasing the cluster mobility. The mechanisms by which these effects are achieved may vary from system to system: unstable first monolayer that causes a sudden nucleation once the necessary coverage is reached as in the case of the Ag-covered surface, strong bonding to the substrate that reduces cluster mobility as in the case of the Au-covered surface, or some mechanisms not encountered or noted in our experiments.

For quasi-FM growth of a system, which in equilibrium is a SK system, two conditions must be fulfilled: (i) the island size at the stage of monolayer completion must be small enough so that the misfit stress-induced 2D-3D transition cannot take place yet[57] or this transition must be hindered by a diffusion barrier onto the monolayer island, and (ii) nucleation and growth of monolayer islands on top of the underlayer may not introduce enough local strain energy to cause a strain-induced 2D-3D transition. Condition (i) is fulfilled when the nucleation rate is very high and the misfit stress small, which can be achieved with a high supersaturation and a compliant substrate. At constant deposition rate this means low temperatures and an interfactant that reduces the rigidity of the substrate. This rigidity reduction by the interfactant is also necessary in order to fulfill condition (ii) because—except for the strain—the growth of the second and following monolayers is basically homoepitaxy. Thus, high density of small islands, limited surface diffusion—phenomena which require strong deviation from thermodynamic equilibrium—and strain relaxation by an interfactant, are responsible for the transition from SK growth at high to FM growth at low temperatures. Purely thermodynamic arguments cannot explain this 2D-3D transition as already pointed out earlier.[58]

To a first approximation an interfactant may be considered as the 2D counterpart to the 3D prenucleation material that has been used already 50 years ago in order to grow thin continuous layers from materials that otherwise would form isolated crystals in the VW growth mode.[59]

V. SUMMARY

We have studied the influence of interfactants on the growth of thin Pb films on the Si(111) surface using low-energy electron microscopy and diffraction. Pb, which grows on the Si(111)-(7×7) surface above 200 K in the Stranski–Krastanov mode, can be induced by suitable interfactants—as exemplified by Au in this paper—to grow in a Frank–van der Merwe-like mode up to 400 K. Within the thickness range studied no critical upper thickness was observed at which the flat film breaks up into 3D crystals as is usually the case with surfactants due to the buildup of stress. Thus, an interfactant apparently not only leads to monolayer-by-monolayer growth but at the same time also relieves misfit stress. The mechanism by which interfactants achieve the desired goal is attributed to enhancement of the nucleation rate and suppression of cluster diffusion.

ACKNOWLEDGMENTS

This work was supported financially by the Deutsche Forschungsgemeinschaft (DFG) and the Bundesministerium für Bildung und Forschung (BMBF, Project No. 05 SL8 WW8-1). Most of the work was done at the Technical University Clausthal. Part of the analysis and of the measurements (Pb/Au-$\sqrt{3}$) was carried out at the Sincrotrone ELETTRA in Trieste, Italy. One of us (T.S.) gratefully acknowledges the Training and Mobility of Researcher (TMR) program of the European Community (Contract No. ERB FMBI-CT 96-1749) for financial support and J. Slezak for experimental assistance. The development of the instrument was supported by the Volkswagen Foundation.

*Author to whom correspondence should be addressed. Present address: Universität Würzburg, Experimentelle Physik II, 97074 Würzburg, Germany. Email: Thomas.Schmidt@physik.uni-wuerzburg.de.

†Present address: Department of Physics and Astronomy, Arizona State University, Tempe, AZ 85287-1504.

[1] E. Bauer, Z. Kristallogr. **110**, 372 (1958).

[2] M. Copel, M.C. Reuter, E. Kaxiras, and R. Tromp, Phys. Rev. Lett. **63**, 632 (1989).

[3] M. Jałochowski and E. Bauer, J. Appl. Phys. **63**, 4501 (1988).

[4] M. Horn-von Hoegen, Appl. Phys. A: Solids Surf. **A59**, 503 (1994); M. Horn-von Hoegen *et al.*, Phys. Rev. B **49**, 2637 (1994), and references therein.

[5] M. Jałochowski, M. Hoffmann, and E. Bauer, Phys. Rev. B **51**, 7231 (1995); Phys. Rev. Lett. **76**, 4227 (1996).

[6] M. Hoffmann, Ph.D. thesis, TU Clausthal, 1996.

[7] H.H. Weitering, D.R. Heslinga, and T. Hibma, Phys. Rev. B **45**, 5991 (1992).

[8] J.A. Carlisle, T. Miller, and T.-C. Chiang, Phys. Rev. B **45**, 3400 (1992).

[9] M. Saitoh, K. Oura, K. Asano, F. Shoji, and T. Hanawa, Surf. Sci. **154**, 394 (1985).

[10] G. LeLay, J. Peretti, M. Hanbücken, and W.S. Yang, Surf. Sci. **204**, 57 (1988).

[11] G. LeLay, in *The Chemical Physics of Solid Surfaces*, edited by D.A. King and D.P. Woodruff (Elsevier, Amsterdam, 1997), Vol. 8 p. 297, and references therein.

[12] P.J. Estrup and J. Morrison, Surf. Sci. **2**, 465 (1964).

[13] G. LeLay, K. Hricovini, and J.E. Bonnet, Appl. Surf. Sci. **41/42**, 25 (1989); Phys. Rev. B **51**, 10193 (1995); G. LeLay, M. Abraham, K. Hricovini, and J.E. Bonnet, in *Kinetics of Ordering and Growth at Surfaces*, edited by M.G. Lagally (Plenum, New York, 1990), p. 209.

[14] G. Quentel, M. Gauch, and A. Degiovanni, Surf. Sci. **193**, 212 (1988).

[15] L. Seehofer, D. Dahoul, G. Falkenberg, and R.L. Johnson, Surf. Sci. **307–309**, 698 (1994).

[16] I.-S. Hwang, R.E. Martinez, C. Liu, and J.A. Golovchenko, Surf. Sci. **323**, 241 (1995).

[17] W. Telieps and E. Bauer, Surf. Sci. **162**, 163 (1985); Ber. Bunsenges. Phys. Chem. **90**, 197 (1986).

[18] ELMITEC Elektronenmikroskopie GmbH, Am Kaiser Wilhelm Schacht 1, D-38678 Clausthal-Zellerfeld, Germany.

[19] E. Bauer, Rep. Prog. Phys. **57**, 895 (1994); Th. Schmidt, S. Heun, J. Slezak, J. Diaz, K.C. Prince, G. Lilienkamp, and E. Bauer, Surf. Rev. Lett. **5**, 1287 (1998).

[20] J.A. Venables, G.D.T. Spiller, and M. Hanbrücken, Rep. Prog. Phys. **47**, 399 (1984).

[21] J.A. Venables, Surf. Sci. **299/300**, 798 (1994); Phys. Rev. B **36**, 4153 (1987).

[22] S. Günther, A. Kolmakov, J. Kovac, M. Marsi, and M. Kiskinova, Phys. Rev. B **56**, 5003 (1997).

[23] G. LeLay, M. Manneville, and R. Kern, Surf. Sci. **65**, 265 (1977); *ibid.* **72**, 405 (1978).

[24] A.A. Saranin, A.V. Zotov, V.G. Lifshits, J.T. Ryu, O. Kubo, H. Tani, T. Harada, M. Katayama, and K. Oura, Surf. Sci. **429**, 127 (1999).

[25] W. Swiech, E. Bauer, and M. Mundschau, Surf. Sci. **253**, 283 (1991).

[26] R. Pless and L.D. Marks, Surf. Sci. **380**, 497 (1997), and references therein.

[27] T. Hasegawa, S. Hosaka, and S. Hosoki, Surf. Sci. **357-358**, 858 (1996).

[28] E.A. Khramtsova, H. Sakai, K. Hayashi, and A. Ichimiya, Surf. Sci. **433-435**, 405 (1999) and references therein.

[29] L. Seehofer, S. Huhs, G. Falkenberg, and R.L. Johnson, Surf. Sci. **329**, 157 (1995).

[30] M. Jałochowski and E. Bauer, Surf. Sci. **213**, 556 (1989).

[31] O. Kubaschewsky and C.B. Alcock, *Metallurgical Thermochemistry* (Pergamon, Oxford, 1979), p. 204.

[32] C.W. Jones, J.M. Marcano, J.K. Norskov, and J.A. Venables, Phys. Rev. Lett. **65**, 3317 (1990).

[33] K. Kyuno, A. Gölzhäuser, and G. Ehrlich, Surf. Sci. **397**, 191 (1998).

[34] E. Bauer, Z. Kristallogr. **110**, 395 (1958), and references therein.

[35] A. Masson, J.J. Metois, and R. Kern, Surf. Sci, **27** 463 (1971).

[36] C. Chapon and C.R. Henry, Surf. Sci. **106**, 152 (1981).

[37] H.D. Velfe, H. Stenzel, and M. Krohon, Thin Solid Films **98**, 115 (1982).

[38] R. Kern, A. Masson, and J.J. Metois, Surf. Sci. **27**, 483 (1971).

[39] H. Reiss, J. Appl. Phys. **39**, 5046 (1968).

[40] G. Kellogg, Surf. Sci. Rep. **21**, 1 (1984).

[41] J.-M. Wen, S.-L. Chang, J.W. Burnett, J.W. Evans, and P.A. Thiel, Phys. Rev. Lett. **73**, 2591 (1994).

[42] J.C. Hamiltan, M.S. Daw, and S.M. Foiles, Phys. Rev. Lett. **74**, 2760 (1995).

[43] J.C. Hamilton, Phys. Rev. Lett. **77**, 885 (1996).

[44] G. Zinsmeister, Vacuum **16**, 529 (1966).

[45] H.D. Velfe and M. Krohn, Thin Solid Films **98**, 125 (1982).

[46] J. Villain, A. Pimpinelli, L. Tang, and D. Wolf, J. Phys. (France) **2**, 2107 (1992).

[47] H. Brune, G.S. Bales, J. Jacobsen, C. Boragno, and K. Kern, Phys. Rev. B **60**, 5991 (1999).

[48] H. Gollisch, Surf. Sci. **175**, 249 (1986).

[49] K.P. Huber and G. Herzberg, *Molecular Spectra and Molecular Structure* (Van Norstrand, New York, 1979), Vol. 4, p. 522, and references therein.

[50] D.W. McComb, D.J. Moffatt, P.A. Hackett, B.R. Williams, and B.F. Mason, Phys. Rev. B **49**, 17 139 (1994).

[51] D.W. McComb, R.A. Wolkow, and P.A. Hackett, Phys. Rev. B **50**, 18 268 (1994).

[52] T. Nakayama, S. Watanabe, and M. Aono, Surf. Sci. **344**, 143 (1995).
[53] L. Seehofer, G. Falkenberg, D. Dahoul, and R.L. Johnson, Phys. Rev. B **51**, 13 503 (1995).
[54] T. Nagao, S. Hasegawa, K. Tsuchie, S. Ino, C. Voges, G. Klos, H. Pfnür, and M. Henzler, Phys. Rev. B **57**, 10 100 (1998), and references therein.
[55] E.A. Khramtsova and A. Ichimiya, Phys. Rev. B **57**, 10 049 (1998).
[56] A.K. Green and E. Bauer, Thin Solid Films **52**, 163 (1978), and references therein.
[57] J.H. van der Merwe and E. Bauer, Phys. Rev. B **39**, 3632 (1989).
[58] E. Bauer and J.H. van der Merwe, Phys. Rev. B **33**, 3657 (1986).
[59] E. Zehender, Optik (Stuttgart) **7**, 200 (1950).